Inter-Research Science Publisher

Marine Ecology Progress Series
Volume 771:105–121

Published October 16, 2025
https://doi.org/10.3354/meps14986

OPEN ACCESS

Challenging traditional methods of age estimation: elemental and isotopic characterisation of speartooth shark *Glyphis glyphis* vertebrae

Hilary M. K. Lewis[1,2,*], Michael I. Grant[2,3], Olivier Alard[1,4], Peter M. Kyne[5], Hui-Qing Huang[6], Yoann Gréau[1], Alastair V. Harry[7], Grant James Johnson[8], Amy Kate Kirke[5,8], Brandon Mahan[9,10]

[1]Research School of Earth Science, College of Science, Australian National University, Canberra, Australian Capital Territory 2601, Australia

[2]Centre for Sustainable Tropical Fisheries and Aquaculture, James Cook University, Townsville, Queensland 4811, Australia

[3]Faculty of Marine Science and Fisheries, Hasanuddin University, Jl. Perintis Kemerdekaan Km.10 Tamalanrea, Makassar 90245, Indonesia

[4]Géosciences Montpellier Pl. Eugène Bataillon, 34090 Montpellier, France

[5]Research Institute for the Environment and Livelihoods, Charles Darwin University, Darwin, Northern Territory 0909, Australia

[6]Advanced Analytical Centre, Research Infrastructure, James Cook University, Townsville, Queensland 4811, Australia

[7]Western Australian Fisheries and Marine Research Laboratories, Aquatic Science and Assessment, Department of Primary Industries and Regional Development Western Australia, Hillarys, Western Australia 6025, Australia

[8]Department of Agriculture and Fisheries, Fisheries Branch, Northern Territory Government, Berrimah, Northern Territory 0828, Australia

[9]Melbourne Analytical Geochemistry, School of Geography, Earth and Atmospheric Sciences, The University of Melbourne, Victoria 3010, Australia

[10]IsoTropics Geochemistry Lab, College of Science and Engineering, James Cook University, Townsville, Queensland 4811, Australia

ABSTRACT: Chondrichthyan (sharks, rays, and chimaeras) age estimation has mostly been informed through counting bands in calcified hard parts such as vertebrae. However, this method is not broadly applicable to all species and is prone to misinterpretation biases. There is a need to improve current age estimation methods, and elemental characterisation of vertebrae is a promising prospect. We analysed vertebrae from speartooth shark *Glyphis glyphis,* a euryhaline species from tropical Australia, by both micro-X-ray fluorescence (μXRF) and laser ablation multi-collector inductively coupled plasma mass spectrometry to discriminate elemental and isotopic variations. Age estimates from μXRF were compared to the conventional ageing method of transmitted light optical microscopy (TLOM). In addition, we investigated ambient environmental changes along the growth axis of vertebrae through *in situ* characterisation of strontium (Sr) isotopic ratios ($^{87}Sr/^{86}Sr$) and conventional solution-based $^{87}Sr/^{86}Sr$ analyses of water samples from the associated habitat. Age estimation through μXRF indicated that Sr exhibits an alternative banding pattern to that of TLOM. This Sr variation is correlated to strong $^{87}Sr/^{86}Sr$ variations, not seen in stenohaline marine species. The elemental and isotopic Sr variation recorded along the growth axis of *G. glyphis* vertebrae is related to the influence of seasonal terrestrial runoff. The predictability of the seasonal rainfall pattern anchors $^{87}Sr/^{86}Sr$ to time and thereby validates Sr bands as annual (between ages 0–11) while it invalidates bands identified via TLOM. This study suggests that detecting elemental and isotopic variations with predictable seasonal fluctuations in a species' ambient environment can provide an alternative means of age validation.

KEY WORDS: Validation · Age and growth · LA-MC-ICP-MS · Life history · Sclerochronology · Biogeochemistry · Biomineralization

*Corresponding author: hilary.lewis@anu.edu.au

Publisher: Inter-Research · www.int-res.com

1. INTRODUCTION

Overfishing of chondrichthyans (sharks, rays, and chimaeras) has resulted in over one-third of all species now being listed as threatened with extinction on the International Union for the Conservation of Nature Red List of Threatened Species (hereafter 'IUCN Red List') (IUCN 2024). Chondrichthyans are particularly susceptible to overfishing due to frequently observed life history characteristics such as slow growth, late attainment of maturity, and low fecundity (Cortés 2000, Grant & Cortés 2024). Being able to estimate age reliably is essential to informing sustainable harvest approaches, population recovery times, and species-specific generational baselines for conservation assessment (e.g. IUCN Red List assessments) (Goldman & Cailliet 2004, Cortés et al. 2024). Calcified hard parts of chondrichthyans (principally vertebrae, but also dorsal spines and caudal thorns, all of which have analogous ageing methods) are the primary structures used in age estimation (Goldman & Cailliet 2004). The elemental analysis of calcified hard parts is still nascent compared to applications to teleost otoliths. As such, there is potential that investigations into their elemental composition could improve reliability of age estimation and additionally offer insights into age-related habitat use (e.g. Hale et al. 2006, Grant et al. 2023).

Visible bands formed in vertebral centra are the primary means for age determination of elasmobranchs (sharks and rays) (Cailliet 2015). Vertebrae are typically sectioned and viewed with transmitted light optical microscopy (TLOM), with the visible band pairs identified as either opaque (summer, high growth density) or translucent (winter, lower growth density); together these are called a band pair and are often assumed to represent 1 annual summer–winter cycle (Cailliet et al. 2006). However, the opacity and translucency of these bands can differ considerably with species and sample preparation methodology (among other variables) and are therefore prone to misinterpretation biases (Campana 2001). Temperate species from regions with a higher magnitude of seasonality tend to have more discrete and distinguishable bands, and species from tropical regions or deep-water tend to lack pronounced temperature-based seasonal changes in their environment, which is attributed to less discrete, difficult to identify band patterns in some cases (Goldman & Cailliet 2004). This creates difficulties and increased subjectivity in age estimation using traditional 'band pairs' identified using TLOM methods (hereafter 'visible bands').

The traditional ageing method of counting visible bands essentially relies upon changes in the density of calcification (e.g. Cailliet & Radtke 1987, Hale et al. 2006) along the growth axis, to the extent that changes can be identified with relatively low-intensity light and a microscope, with occasional use of staining techniques to enhance visualisation (Goldman & Cailliet 2004). This ageing technique follows ring band counting of teleost otoliths, and some species of shark and ray have had the temporal periodicity of band pair depositions validated (e.g. McFarlane & Beamish 1987, Simpfendorfer et al. 2002) or indirectly verified (e.g. Hall et al. 2012). However, only a few species have been reliably aged, and for some species, no visible banding pattern is detected (e.g. Burke et al. 2020). For other species, a visible banding pattern is detected that does not correlate with annual seasonal cycles, suggesting that changes in calcification density may rather have a more structural morphological function (e.g. Natanson et al. 2018). Furthermore, visible bands become increasingly small, compacted, and difficult to read in adult age classes, and calcification may cease in large adults, leading to concerns that counting of visible bands has led to a systematic underestimation of longevity (Harry 2018). Taken together, this calls for a need to explore alternative methods and techniques to estimate age.

One avenue to improve accuracy and precision of age estimates is through analysis of elemental concentrations along the growth axis, which may allow a wider range of species to be reliably aged (Scharer et al. 2012). Various trace elements are incorporated into calcified hard parts of sharks and rays, through either substitution with Ca in phosphate hydroxyapatite [$Ca_{10}(PO_4)_6(OH)_2$], or through entrapment in the supporting protein matrix (see McMillan et al. 2017 for further discussion). Several of these trace elements passively enter the body via diffusion across the gills (or other exposed soft tissues), and their concentration within calcified hard parts reflects the elemental and isotopic composition of the ambient environment at the time of accretion (e.g. Tillet et al. 2011, Smith et al. 2013, Grant et al. 2023). A relatively unexplored application of analysing elements in vertebrae is whether known annual changes in ambient environmental element profiles can be used in the context of ageing (e.g. Scharer et al. 2012). This could be useful for species that occur in regions with highly predictable seasonal rainfall or temperature cycles, and where particular elements or their isotopic ratios are known to be influenced by such robustly periodic inputs.

This study aims to demonstrate that known chemical changes that are linked to seasonal environmental processes can offer a means of age validation and reduce reliance on variably effective counts of visible bands

via TLOM ageing methods. In this context, strontium (Sr) concentrations and radiogenic Sr isotope ratios—$^{87}Sr/^{86}Sr$—have proven to be particularly useful in distinguishing between chemically distinct water bodies, such as the freshwater to marine spectrum (Hegg et al. 2013). This is because oceanic water has a distinct $^{87}Sr/^{86}Sr$ ($^{87}Sr/^{86}Sr_{SW}$ = 0.709167 ± 0.000009; $[Sr]_{SW}$ 7.8 µg g^{-1}) (Veizer 1989, Zaky et al. 2019) while freshwater $^{87}Sr/^{86}Sr$ is dependent on the age and geological characteristics of the river basin catchment, along with precipitation, whereby runoff leaches Sr from the catchment geology and into the river. Therefore, there is potential to analyse calcified hard parts of sharks and rays occurring in a river environment to quantify seasonally predictable changes in terrestrial runoff through corresponding changes in $^{87}Sr/^{86}Sr$ ratios along the growth axis. Sr readily substitutes for Ca in apatite without isotopic fractionation, providing an alternative ageing technique through the quantification of dry and wet seasons an individual has lived through.

Modern analytical platforms, namely here multi-collector inductively coupled plasma mass spectrometry (MC-ICP-MS), have increased capacity to reveal such fine-scale chemical contrasts (isotopes), while preserving high spatial resolution (Chew et al. 2021). Laser ablation (LA-ICP-MS) has been used for *in situ* analysis of elements in biological samples including shark and ray teeth, vertebrae, and dorsal fin spines (e.g. McMillan et al. 2017). Studies that have used LA-ICP-MS to make ecological movement inferences have observed robust temporospatial variations in elemental patterns, yielding promising results for a number of species (McMillan et al. 2017), including the shark samples analysed herein (Grant et al. 2023). The advantages of MC-ICP-MS over ICP-MS arise from its ability to achieve high precision isotope ratio measurements with lower associated analytical uncertainties. This capability is particularly valuable for applications focusing on isotope ratio analysis, rather than elemental concentrations, which are typically measured using quadrupole ICP-MS. Therefore, there is scope to conduct a high-precision analysis on Sr isotope ratios, to examine changes along the growth axis of vertebrae using *in situ* LA-MC-ICP-MS techniques. Meanwhile, the analytical resolution of micro-X-ray fluorescence (µXRF) is constrained to elements that are relatively high in concentration, but this technique may have complementary value for broader, rapid analysis of Sr concentrations (e.g. Raoult et al. 2016).

Here, we focused on the speartooth shark *Glyphis glyphis* (listed as Vulnerable on the IUCN Red List, Kyne et al. 2021a), a euryhaline species that occupies rivers of tropical Australia and New Guinea. While its life history is poorly known, ecologically, this species prefers turbid water, with immature individuals occupying riverine environments based on tidal and seasonal freshwater flow regimes. Adults appear to occur mostly in lower estuary environments or run-off-influenced coastal zones (Pillans et al. 2009, Dwyer et al. 2020, Grant et al. 2023). In this study. we investigated the use of $^{87}Sr/^{86}Sr$ characterisation in both water samples and vertebrae of *G. glyphis* from the Adelaide River, Northern Territory, Australia, while coupling these data to µXRF elemental profiles. The Adelaide River terrestrial and aqueous catchment $^{87}Sr/^{86}Sr$ ratio has been well characterised previously, showing strong seasonal $^{87}Sr/^{86}Sr$ compositions reflective of the region's highly seasonal rainfall, and freshwater $^{87}Sr/^{86}Sr$ ratios show a pronounced departure from the stable oceanic average $^{87}Sr/^{86}Sr$ ratios (de Caritat et al. 2023). We hypothesised that quantification of changes in Sr concentration and $^{87}Sr/^{86}Sr$ ratios along the growth axis of vertebrae will allow a means of validated age estimation, as Sr concentration and $^{87}Sr/^{86}Sr$ changes in the environment are linked to rainfall events and thus can be fixed to time based on the Northern Territory's predictable and pronounced annual wet and dry season.

The specific aims of this study were to:

(1) Investigate the elemental composition and distribution of elements (Ca, P, K, and Sr) within vertebrae of *G. glyphis* and marine reference species (*Carcharhinus coatesi*) using µXRF, compared to bands identified through the TLOM ageing method.

(2) Measure the $^{87}Sr/^{86}Sr$ isotopic compositions of water along a transect of the Adelaide River to geochemically characterise the environment of *G. glyphis* and discuss the factors driving isotopic and compositional variations.

(3) Determine the Sr isotopic ratios along the growth transect of *G. glyphis* vertebrae and compare these ratios to those of marine species.

(4) Evaluate the similarity between time-series rainfall patterns and the variability in $^{87}Sr/^{86}Sr$ compositions along the growth transects of *G. glyphis* vertebrae, and explore the potential of this method for age validation.

2. MATERIALS AND METHODS

2.1. Sample collection

Glyphis glyphis samples (n = 10; 59.8—189 cm total length) were collected from the Adelaide River during targeted surveys in 2015—2016 (Kyne et al. preprint https://doi.org/10.1101/2022.09.26.509619). Sharks

Table 1. Catch information for speartooth sharks *Glyphis glyphis* collected from the Adelaide River, Northern Territory, Australia, and their assessed transmitted light optical microscopy (TLOM) ages, their micro-X-ray fluorescence (μXRF) ages based on elemental profiles, and strontium (Sr) isotope data from laser ablation multi-collector inductively coupled plasma mass spectrometry (LA-MC-ICP-MS) (values are averages from transects after the birth mark) with associated SD. Readability scores ranged from 1 to 5, with 1 being unreadable and 5 being the easiest to decipher. NA: no age deciphered

Assigned ID	Catch date	Longitude (°E)	Latitude (°S)	Distance upstream (km)	Salinity (ppt)	Length (cm)	Sex	TLOM age (yr)	TLOM readability	μXRF age (yr)	μXRF readability	Sr (ppb)	SD	$^{87}Sr/^{86}Sr$ ratio	SD
1	Dec 2015	131.39429	12.50701	67	19.06	144.5	F	6	3	6	3	2437.0	431.4	0.709175	0.0002279
2	Dec 2015	131.39429	12.50701	67	19.06	101.5	M	4	2	NA	1	2375.1	95.8	0.709188	0.0003346
3	Dec 2015	131.39415	12.50701	67	17.21	127	F	6	2	6	2	1792.2	241.1	0.709221	0.0005985
4	Dec 2015	131.39415	12.50701	67	17.21	80.1	F	1	4	1	4	2506.0	199.3	0.709229	0.0004336
5	Nov 2015	131.28258	12.75479	110	4.04	59.8	F	0	5	0	4	2376.2	189.3	0.709325	0.0002352
6	Dec 2015	131.37001	12.47871	59	15.37	139.5	M	5	5	3	5	2263.2	393.1	0.709577	0.0018003
7	Dec 2015	131.39406	12.50696	67	12.12	153.2	M	8	2	7	3	2419.2	253.0	0.740949	0.0005208
8	Oct 2016	131.33289	12.67560	96	5.05	189	F	10	5	7	5	2122.1	258.8	0.755616	0.0009577
9	Nov 2016	131.29323	12.69685	101	4.15	181.5	F	11	4	10	4	2194.1	264.2	0.749025	0.0012770
10	Nov 2016	131.33482	12.68193	96.5	6.29	161	F	8	4	8	4	1458.1	213.2	0.712928	0.0015845

were collected in riverine environments at salinities of 4.0–19.1 ppt (Table 1). To assist in the interpretation of results, we included a vertebra sample of the northern river shark *G. garricki* from Western Australia as an additional riverine species in an alternate location (collected by the Western Australian Department of Primary Industries and Regional Development), and samples of the Australian blackspot shark *Carcharhinus coatesi* from marine waters of Van Diemen Gulf where the Adelaide River drains (Kirke et al. 2024).

To firstly determine whether $^{87}Sr/^{86}Sr$ are incorporated into calcified hard parts in the same ratio as the ambient environment, samples from stenohaline marine species were used to analyse their internal $^{87}Sr/^{86}Sr$ ratios against the known marine water values. We used species highly removed from river runoff: shortnose spurdog *Squalus megalops* vertebrae that were obtained from the bycatch of deepwater commercial prawn trawlers operating in the Queensland east coast otter trawl fishery in 2011 (Rigby et al. 2016); silky shark *C. falciformis* that were collected offshore in Papua New Guinea (Grant et al. 2018); and teeth from the scalloped hammerhead *Sphyrna lewini* that were obtained from the jaw of a specimen from northern New South Wales that was kept at James Cook University (JCU; Townsville, Queensland, Australia) (Heupel et al. 2020). We also included *C. coatesi* as a marine species that may be influenced by river runoff in this analysis.

Thoracic vertebrae were removed from each animal and stored frozen. In the laboratory, excess cartilage was manually removed and vertebrae were dried for use in age estimation, after which they were stored in sealed containers (further details can be found in their associated studies cited above). Dried vertebrae were sent to JCU, where they had any remaining tissue manually removed before being stored in sealed containers before preparation for analysis.

2.2. Sample preparation

Dried vertebrae were embedded in 2-part epoxy resin (EpoFix®, Struers) in 2.54 cm (1 inch) silicone mounts, sagittally sectioned and polished to achieve a uniform thickness. *S. lewini* teeth were rinsed in ultrapure Merck Millipore Milli-Q® 18Ω water (hereafter MQ water) before being dried at 40°C in a vented oven for 12 h before similarly being mounted using a 2-part epoxy resin (EpoFix®, Struers) in 2.54 cm round moulds. Before curing, all samples were placed into a vacuum chamber for 10 min at 0.1 bar (100 hP) to ensure adequate gas removal and proper resin impregnation; samples that experienced continued outgassing after 10 min were re-processed through the vacuum stage until outgassing visibly ceased. Mounted samples were then cured in a 40°C oven for 12 h. After curing, mounted samples were polished to a 1 μm polish (diamond suspension). Samples were rinsed with MQ water, sonicated, and air-dried prior to laser ablation.

2.3. Age determination

Ages were previously estimated for *G. glyphis* (Kyne et al. preprint https://doi.org/10.1101/2022.09.26.509619) using TLOM methods as per Goldman & Cailliet (2004). Visible band pairs corresponding to these age estimates were reidentified in the present study.

We identified the birthmark for all vertebrae examined as the acute change in angle on the inner margins of the corpus calcareum, representing the shift from embryonic development to post-natal growth (Goldman & Cailliet 2004).

2.4. μXRF

For semi-quantitative element mapping, prepared vertebrae sagittal sections were placed in the vacuum chamber (0.1 atm) of a Bruker M4 Tornado μXRF, and the spatial distribution of the following elements was analysed: K, Ca, Sr, P. The X-rays were focused to 20 μm using polycapillary X-ray optics. Multi-element maps were acquired at 50 kV and 600 μA. The pixel step was 20 μm. An acquisition time of 8 ms per pixel (2.5 mm s^{-1}) and 3 cycles were used to map the entire vertebrae. The approximate analysis time of each vertebral section was 4 h. Two readers independently counted bands on elemental maps of vertebrae. Each elemental map was read by the first reader (H. M. K. Lewis) and then by an experienced second reader (M. I. Grant). Each sample was assigned a readability score (Table 1), with 1 being unreadable and 5 being the easiest to decipher. An age was recorded when counts were agreed upon (Table 1), and consensus reads were conducted where age estimates differed between readers, which is the standard method of age estimation (e.g. Grant et al. 2018, Kirke et al. 2024, Kyne et al. preprint https://doi.org/10.1101/2022.09.26.509619).

2.5. Natural waters

Surface water samples were collected at 10 sites along a salinity gradient from the marine waters of Adam Bay to freshwater reaches of the Adelaide River (Table 2, Fig. 1). Latitudinal and longitudinal coordinates (WGS84) were recorded at each site along with salinity using a handheld Qanta water quality meter.

Water samples were collected in acid-washed/cleaned (3 wk in 2 mol l^{-1}, M, double distilled nitric acid, HNO_3) 1 l polypropylene (PP) bottles, kept refrigerated, and transported cold from the collection site to the IsoTropics Geochemistry Lab at JCU. To stabilise water samples for storage and further analyses, upon receipt in the lab, samples were filtered using 50 ml PP syringes and 0.45 μm hydrophilic polytetrafluoroethylene (PTFE) filters (Microscience Hydraflon™ 35 mm diameter syringe filters; rinsed and purged using high-purity MQ). Water filtrates were collected into 400 ml acid-leached PP containers (2M HNO_3 double distilled for 3 wk). Post-filtration water samples were then acidified to 2% using double-distilled 16M HNO_3 to arrest the formation and propagation of precipitates or organics.

Sr separation chemistry was conducted in the IsoTropics Geochemistry Laboratory, following established separation protocols (Charlier et al. 2006). Sr isotope compositions were measured with a ThermoFisher® Neptune™ MC-ICP-MS at the Advanced Analytical Centre (AAC; JCU). The interface system consisted of a standard Ni sample cone and H-skimmer cone, and the introduction system consisted of a double-pass dual cyclonic spray chamber (Glass Expansion™) coupled to an Elemental Scientific® PFA-ST nebuliser with 100 μl min^{-1} probe-capillary assembly. Each analysis was preceded by a 90 s wash out and 50 cycles of 4.194 s integrations with static Faraday collectors. Analytical procedural blanks were <100 pg Sr and are negligible relative to the amount of Sr processed (typically greater than 600 ng). All results were mass-bias corrected using

Table 2. Sample location and field information for water samples collected from the Adelaide River, Northern Territory, Australia. Standard error (2SE) is reported for $^{87}Sr/^{86}Sr$ ratios and propagated

Water sample ID	Latitude (°S)	Longitude (°E)	Salinity (10^{-12} g g^{-1})	Elevation (m)	Distance Upstream (km)	$^{87}Sr/^{86}Sr$	2SE (propagated)	^{88}Sr (ppb)
AR1	12.18858	131.19949	38.5	0	0	0.709175	0.000010	785
AR2	12.18534	131.22403	38.3	0	1	0.709188	0.000009	817
AR3	12.22806	131.25108	38.1	0	8.3	0.709221	0.000008	803
AR4	12.39535	131.31694	30.2	4	32	0.709229	0.000010	632
AR5	12.44335	131.32901	20.2	10	46.2	0.709325	0.000007	403
AR6	12.48215	131.36395	10.1	16	60.3	0.709577	0.000013	197
AR7	13.24021	131.10783	0.14	54	195	0.740949	0.000020	1.37
AR8	13.09274	131.23424	0.12	31	167	0.755616	0.000019	1.55
AR9	12.92719	131.26556	0.15	14	143	0.749025	0.000018	2.12
AR10	12.66101	131.33636	0.64	5	94.5	0.712928	0.000022	15.2

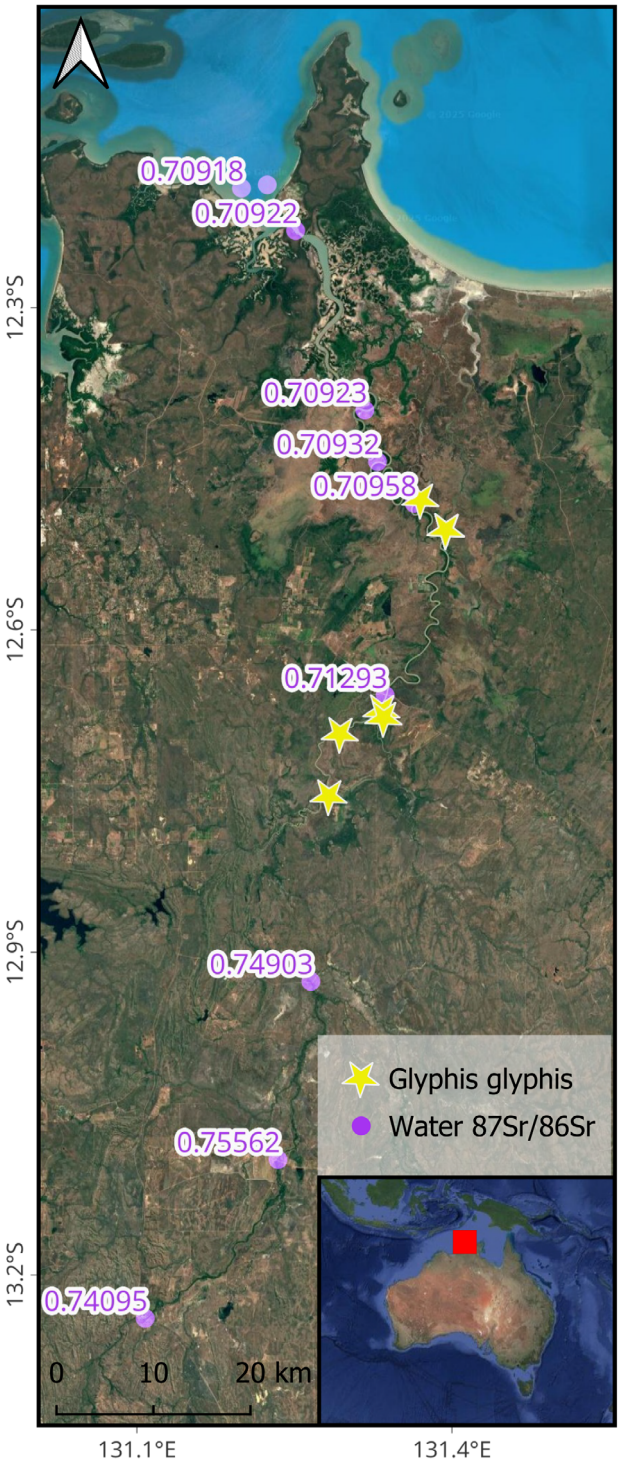

Fig. 1. Water sample collection sites in the Adelaide River, Northern Territory, Australia, and their associated strontium isotope ratios, with speartooth shark *Glyphis glyphis* catch locations indicated by stars

NIST SRM 987 ($^{87}Sr/^{86}Sr$ = 0.710248, McArthur et al. 2001) (analysed at the beginning and end of every sequence, and every second sample); analytical uncertainties are reported conventionally as 2 times the internal standard error (2SE). As a quality assurance metric for long-term reproducibility, the Certified Reference Material NASS-7 (National Research Council of Canada, NRC) was processed and analysed alongside natural water samples and remained within 2SE ± 0.000018 of the reported value (Phan et al. 2021).

2.6. LA-MC-ICP-MS

Sr isotope analysis ($^{87}Sr/^{86}Sr$) methods described by Vroon et al. (2008) were employed. *In situ* mass spectrometric analysis of vertebrae was conducted at the AAC using a Teledyne Analyte G2 193 nm ArF Excimer laser ablation system connected to a ThermoFisher® Neptune™ MC-ICP-MS using Ni sample cone and Ni X-cone, Tygon tubing for aerosol path, and a 3-way mixing bulb. The sample gas was He with N_2 carrier gas. A spot size of 85 µm, fluence of 3 J cm^{-2}, and repetition rate of 5 Hz were used. Data were treated using the iolite V4 Data Reduction Software (DRS) package outlined by Mulder et al. (2023). Analytical sessions consisted of instrument and analytical optimisation using National Institute of Standards (NIST) 610 (Glass) for signal optimisation, and Mt McClure Apatite reference standard (MRG-1), Madagascar Apatite reference standard (MAD-1), and NanoSr as reference materials to ensure accuracy of $^{87}Sr/^{86}Sr$ results. A standard bracketing approach was employed to measure and correct for instrumental drift over time with a range of Sr concentration standards measured every 5 samples.

3. RESULTS

3.1. µXRF elemental profiles

Of the elements analysed, only Ca, K, P, and Sr were used in visualising banding. Sr and Ca produced distinct banding of varying interpretation levels, while K and P did not produce decipherable banding themselves but assisted in the interpretation of Sr and Ca banding through composite false-colour imaging (Fig. 2). In some instances, age estimates could not be determined using Ca (either alone or in a composite image) due to low interpretability (Fig. S1 in the Supplement at www.int-res.com/articles/suppl/m771p105_supp.pdf). As such, Sr µXRF banding was prioritised for further interpretation in the current work.

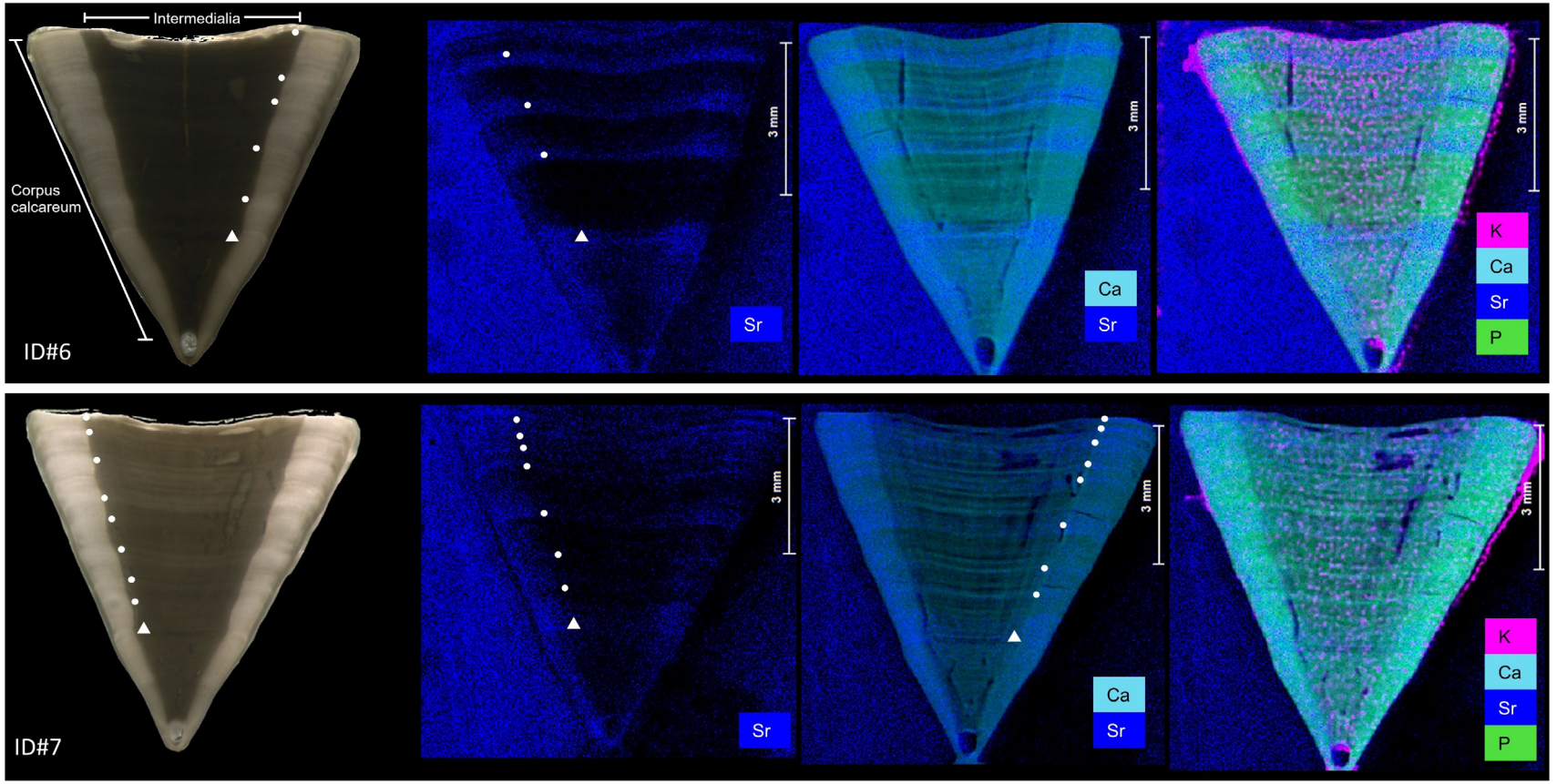

Fig. 2. Differing age estimates for 2 speartooth sharks *Glyphis glyphis* (top: 139.5 cm total length [TL], male, assigned ID6 in Table 1; bottom: 153.2 cm TL, male, ID7 in Table 1) sagittal vertebral sections under transmitted light optical microscope (left; panel 1) and micro-X-ray fluorescence (μXRF) (panels 2–4). Visible age bands are denoted with a white circle, and birth mark is denoted by the first white triangle. μXRF images show multiple layered elements (panel 2: strontium; panel 3: calcium strontium composite; panel 4: potassium, calcium, strontium, and phosphorus composite); ages were derived from Sr intensity (panel 2). Further μXRF images can be found in Fig. S1

The comparison of µXRF and TLOM to age spear-tooth shark vertebral sections provided varying estimates (Fig. 2; Fig. S1). Age estimates were generally lower when determined through µXRF images using Sr (either alone or in a composite image, Fig. 2) compared to TLOM (Fig. 3). Discrepancy was higher for age estimates >8 yr. In some instances, µXRF and TLOM gave equal age estimates, although the position of visible bands in TLOM and Sr bands in µXRF images were not congruent along the growth axis. On average, µXRF age estimates were 1.3 ± 1.3 yr (SD) lower than TLOM, and the agreement of TLOM and µXRF age estimates decreased with increasing age.

For the marine reference species, the Australian blackspot shark (inshore marine), visible band pairs were difficult to interpret using TLOM (Fig. S2), and the use of µXRF imagery (both Ca and Sr) did not enhance band visibility.

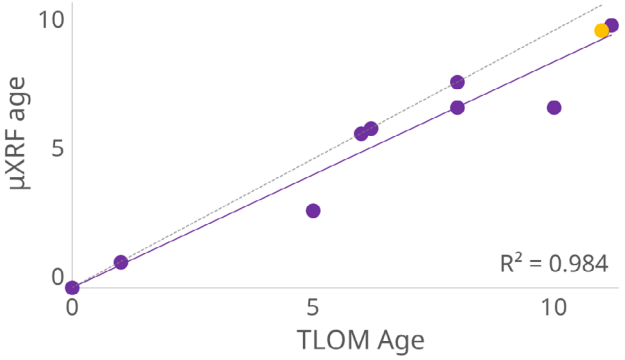

Fig. 3. Comparison of age data, where transmitted light optical microscopy (TLOM) ageing was completed conventionally as per Kyne et al. (preprint https://doi.org/10.1101/2022.09.26.509619). Micro-X-ray fluorescence (µXRF) ages were achieved by counting strontium bands on false colour imagery following analysis, as per Fig. 2. Further ageing analysis for all species in Fig. S1. Purple dots: *Glyphis glyphis* (9 of 10 samples shown, as Assigned ID2 [see Table 1] could not be aged with µXRF); yellow dot: *G. garricki*. The aged shark trendline (purple) compared to the 1:1 line (grey dashed line)

3.2. River water

Using surface water elemental and isotopic $^{87}Sr/^{86}Sr$ analysis enabled us to establish an isotopic reference data set across a substantial section of the Adelaide River system including where *Glyphis glyphis* samples were obtained for the current study (Table 2, Fig. 1). The river Sr concentration increased (0.0155 to 0.817 µg g^{-1}) downstream into estuarine areas, in agreement with marine reference values (Crook et al. 2017). The river mouth and coastal Sr isotope values (~0.70917 ± 0.0001) are congruent with a modern marine $^{87}Sr/^{86}Sr$ value of 0.70918 ± 0.00001 (Veizer 1989). With increasing distance inland, the river water became more radiogenic upstream ($^{87}Sr/^{86}Sr$ increases), concomitant with lower Sr concentration. The Sr concentration and isotopic composition of the river water samples are well reproduced using a mixing model (Fig. 4) between 2 endmembers: seawater ($[Sr]_{SW}$= 7.8 µg g^{-1}, $(^{87}Sr/^{86}Sr)_{SW}$ = 0.70919) and river water containing dissolved crustal Sr (DCSr) from the riverbed and catchment rocks ($[Sr]_{DCSr}$ = 0.001 µg g^{-1}, $(^{87}Sr/^{86}Sr)_{DCSr}$ = 0.76) A conceptual model illustrates how this would change seasonally (Fig. 5).

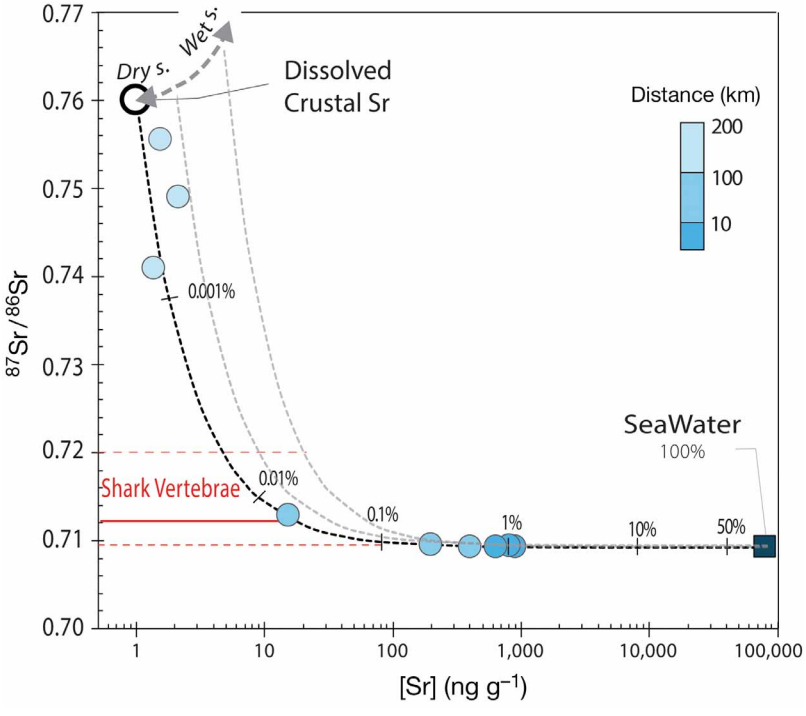

Fig. 4. Mixing model between seawater and river water. Blue circles are water samples along the Adelaide River, Northern Territory, Australia; blue shades denote distance to coast (0–10, 10–100, 100–200 km; see colour key). Tick marks and associated percentages denote the proportion of seawater components (in %). Red solid line denotes the median $^{87}Sr/^{86}Sr$ composition of the shark vertebrae studied here, while lower and upper dashed lines are the maximum and minimum compositions, respectively. Seawater: $[Sr]_{SW}$ = 7.8 µg g^{-1}; $(^{87}Sr/^{86}Sr)_{SW}$ ≈ 0.7092; Veizer 1989); river water for which dissolved crustal Sr (DCSr) is mainly sourced from the Pine Creek geological area, a Paleo-Mesoproterozoic-formation($[Sr]_{DCS}$ =1 ng g^{-1}; $(^{87}Sr/^{86}Sr)_{DCS}$ ≈ 0.76; de Caritat et al. 2023). Dry s.: dry season; Wet s.: wet season

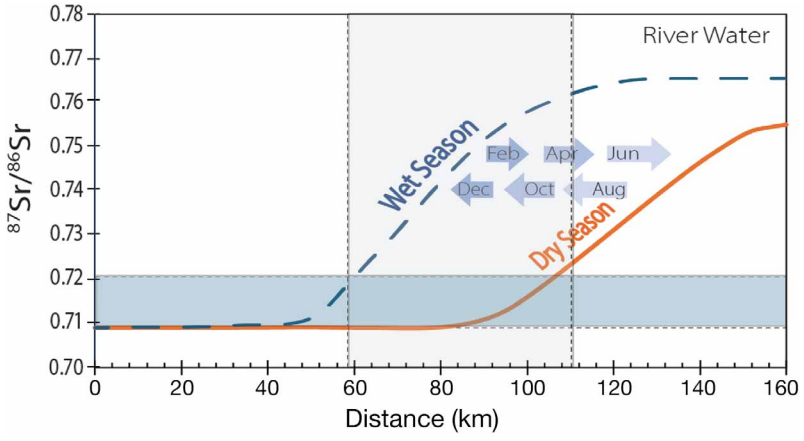

Fig. 5. Conceptual model illustrating the seasonal variation in strontium (Sr) isotope composition of river water by distance (km) from river mouth. The solid curve represents the measured (Table 2) and modelled (Fig. 4) composition of Adelaide River water during the dry season. The dashed blue curve shows the expected composition of the river water based on the seasonal variation observed in the nearby Daly River (Crook et al. 2017); refer to Section 4.2 for further details. Minimum and maximum sampling locations and Sr isotope values of the shark individuals are also depicted using grey dashed lines. As rainfall increases during the wet season, the washout of radiogenic Sr from surrounding rock basements rises, pushing the Sr front downstream, closer to the sea (refer to Section 3.2 for further details). When precipitation decreases, the Sr front shifts back to an upstream position

3.3. *In situ* $^{87}Sr/^{86}Sr$ ratios

Of the calcified hard parts from the stenohaline marine species analysed, we found that $^{87}Sr/^{86}Sr$ values varied from the global marine average by only +0.000022 for the *Sphyrna lewini* teeth (±0.000038 SD) to −0.000062 for the *Squalus megalops* vertebrae (±0.000049 SD) (Table S1), i.e. very little deviation from seawater $^{87}Sr/^{86}Sr$ ratios in part encompassed by analytical uncertainty. The $^{87}Sr/^{86}Sr$ values along the growth axis of *Carcharhinus coatesi* and *C. falciformis* remained steady around the marine ratio (±0.00008 and 0.000065 SD, respectively), largely independent of the variations in Sr intensity (Table S1).

For *G. glyphis*, median $^{87}Sr/^{86}Sr$ values differed along the vertebral growth axis, with values ranging between 0.7091 (marine) and 0.7556 (riverine) (Table 1). Considering results from the river water characterisation (Table 2, Fig. 1), $^{87}Sr/^{86}Sr$ values in vertebrae provided no evidence for strictly marine or freshwater environmental signatures within the vertebrae. All *G. glyphis* vertebral transect $^{87}Sr/^{86}Sr$ averages in the postnatal region (average, 0.712146 ± 0.0015) were significantly above the marine ratio. Pre-natal growth $^{87}Sr/^{86}Sr$ averages ranged between 0.709 and 0.712. In all individuals, there was a sharp increase in $^{87}Sr/^{86}Sr$ ratios moving from the pre-natal growth zone across the birthmark into postnatal growth (e.g. from 0.7110 to 0.7140; Fig. 6)

The variation in Sr intensity from µXRF was in agreement with the variation in Sr voltage obtained by LA-MC-ICP-MS and inversely correlated to $^{87}Sr/^{86}Sr$ ratios (Fig. 6). High Sr intensity bands in µXRF images had higher Sr concentration and lower $^{87}Sr/^{86}Sr$ values determined by LA-MC-ICP-MS, while low Sr intensity bands had lower Sr concentration and higher $^{87}Sr/^{86}Sr$ values. The fluctuations in $^{87}Sr/^{86}Sr$ (and Sr voltage) provide better analytical resolution and finer detail than µXRF (Fig. S3).

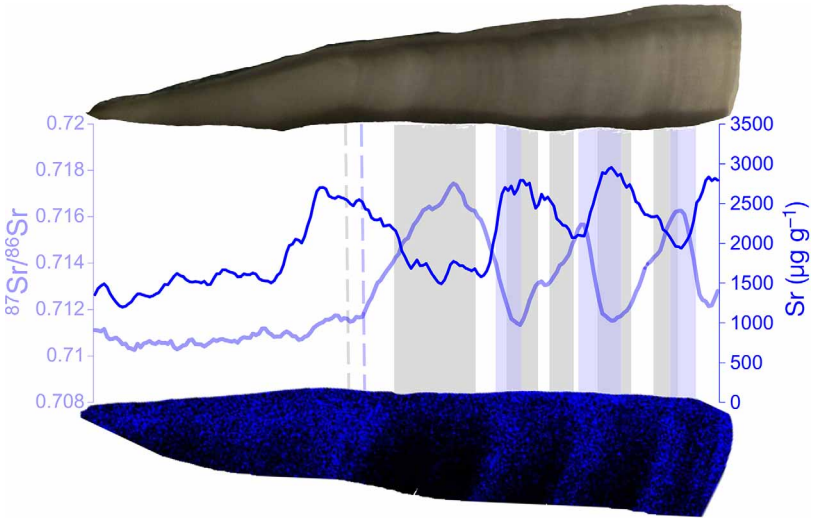

Fig. 6. Sample ID6 speartooth shark *Glyphis glyphis* from the Adelaide River, Northern Territory, Australia, laser ablation data across a transect of the corpus calcareum travelling distally from the centrum. The top image shows transmitted light optical microscopy (TLOM) with visible opaque bands identified by the grey bars; the grey dashed line identifies the birthmark. The bottom depicts micro-X-ray fluorescence (µXRF) false colour imagery showing strontium intensity; the blue bars indicate the identified ageing bands; the blue dashed line identifies the birthmark. Analytical uncertainties sit within the thickness of the line. This sample was aged as 5 yr old using TLOM in the present study and by Kyne et al. (preprint https://doi.org/10.1101/2022.09.26.509619)

Relating to *in situ G. glyphis* transect seasonality, peaks in Sr concentration, $^{87}Sr/^{86}Sr$ ratios, and local precipitation can be used to establish correspondence between individual shark vertebrae relative to rainfall (Fig. 7). Individuals ID8, ID9, and ID10 (Fig. 7) were sampled in October and November 2016, ~96–101 km upstream (Table 1), within the estuarine section of the river most affected by the wet season 'Sr-pulse' (see Fig. 4). The correspondence between $^{87}Sr/^{86}Sr$ and Sr peaks and troughs and the rainfall follows the rationale summarised in Figs. 4 & 5, where wet seasons are marked by radiogenic Sr composition and low Sr concentration, while dry seasons are characterised by more marine Sr ($^{87}Sr/^{86}Sr \approx 0.709$) isotopic and elemental composition (seen in Fig. 7) as the seawater wedge ingress upstream is at its maximum.

4. DISCUSSION

The present examination of vertebrae provided strong evidence that ambient $^{87}Sr/^{86}Sr$ ratios are incorporated into calcified structures in ratios consistent with the ambient environment through seasonality of rainfall. Here we discuss the potential to use these signatures as a means of validating age estimation. To build this case, we discuss (1) μXRF maps and their utility for ageing, (2) the characterisation of riverine isotope development, (3) the analysis of Sr isotopes within vertebrae and their linkage to observed rainfall, and (4) the implications of these findings for age estimations in *Glyphis glyphis*, and broader applications to sharks and rays in general.

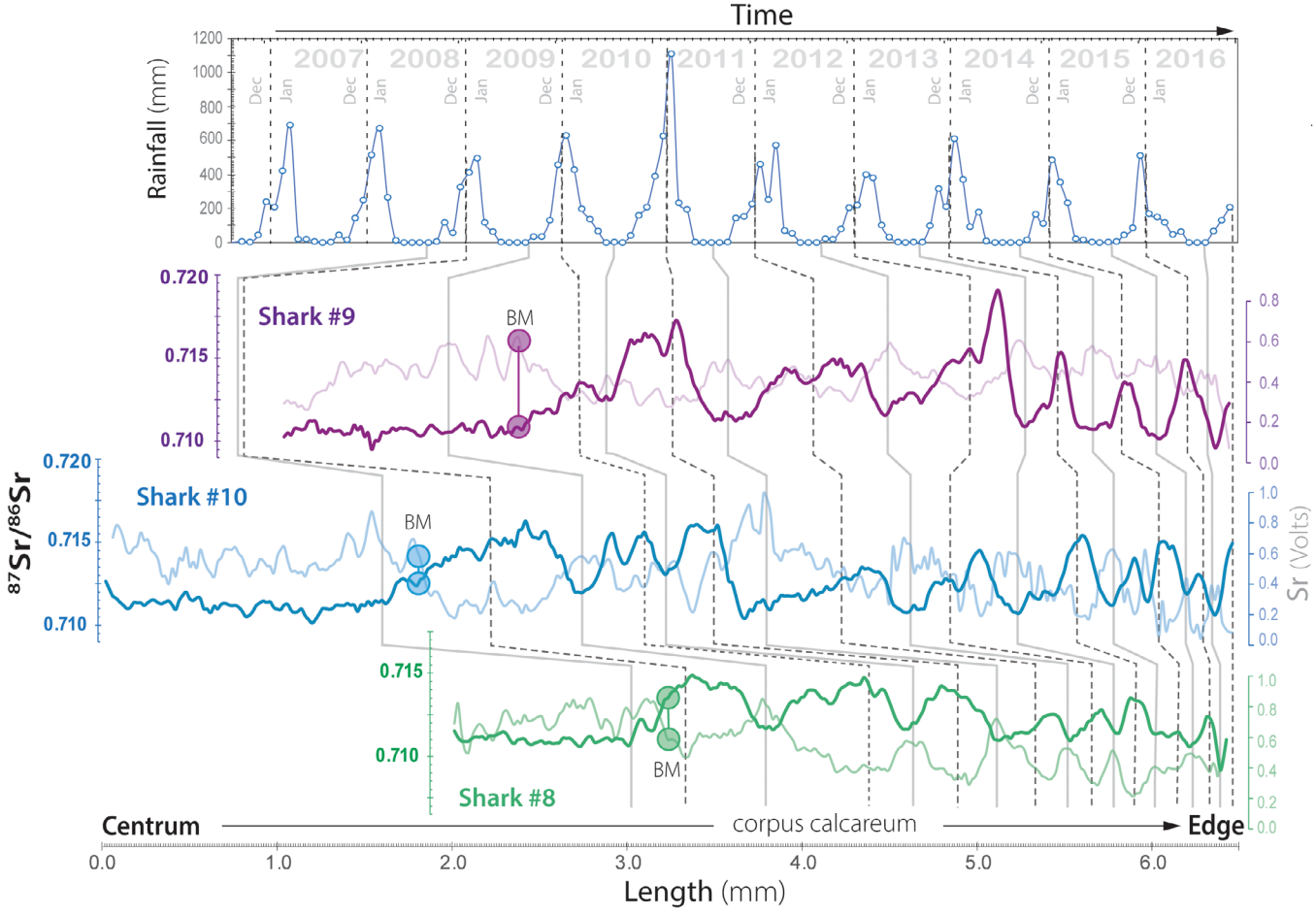

Fig. 7. (Top) Average monthly precipitation (in mm) from October 2006 to November 2016 measured at Darwin International Airport, obtained from the Australian Bureau of Meteorology (www.bom.gov.au/climate/cdo/about/cdo-rainfall-feature.shtml). The rainfall peaks between November and April correspond to the wet season. Laser ablation multi-collector inductively coupled plasma mass spectrometry (LA-MC-ICP-MS) transects for speartooth shark *Glyphis glyphis* individuals ID9, ID10, and ID8, with identified birthmarks (BM), are shown. **Bolded** lines denote $^{87}Sr/^{86}Sr$ ratios, while the light lines correspond to strontium (Sr) intensity (given in volts) and are directly proportional to Sr concentration. Vertical dashed lines indicate the beginning of the year, which broadly corresponds to the onset of the wet season. Solid grey lines indicate dry season records

4.1. μXRF elemental age estimates

Differences were observed between the number and positioning of Sr bands and visible band pairs in vertebrae of *G. glyphis* and the single *G. garricki* specimen. This implies that visual banding and Sr banding are related to different processes and only occasionally coincide for reasons that are presently not understood. This contrasts previous investigation of μXRF conducted on vertebrae of stenohaline marine species, where Sr banding was congruent with visual banding, suggesting that physiological (animal growth) or environmental factors leading to changes in density of calcification and Sr incorporation in vertebrae are similar in marine environments (Raoult et al. 2016). The difference between this and the present study could be related to the differences in marine and river environments, with Sr being highly dynamic in the latter. The disparate banding pattern between Sr and visual bands in the present study appears to be due to the seasonally dynamic ambient concentration of Sr in the estuarine environment of *G. glyphis*, which is discussed further within the Sr isotope interpretations in Section 4.3.

In the present study, μXRF and $^{87}Sr/^{86}Sr$ ratios were found to assist identification of the birthmark. This supports observations that elemental characterisation can be useful for determining the transition from prenatal to post-natal growth in vertebrae (Raoult et al. 2018, Grant et al. 2023) and may have useful applications to minimise subjectiveness in birthmark identification. For *G. glyphis* and *G. garricki*, a low intensity μXRF Sr band and low MC-ICP-MS Sr voltage (i.e. low Sr concentration) occurred immediately after the birthmark (and the $^{87}Sr/^{86}Sr$ ratio was higher, e.g. Fig. 6), indicating that pupping occurs at the early onset of the wet season, in accord with field observations of the pupping season in Australia and New Guinea (October–December; Pillans et al. 2009, Grant et al. 2021). While vertebrae from adult *G. glyphis* were not available for this study, we also found that bands at the distal edge were easier to interpret with μXRF in comparison to TLOM (likely due to higher signal fidelity in μXRF relative to optical light transmission). Resolution at the distal edge of vertebrae under TLOM is challenging, as visible bands become smaller, more compressed, and the opaque-translucent pattern can be hard to distinguish optically and by the human eye. This is a contributing factor to underestimation of older age classes across sharks and rays (Harry 2018), and future research is needed to assess the effectiveness of elemental characterisation in assisting band pair identification at the distal edge of large adults.

4.2. Characterisation of Adelaide River water

The Sr composition ($^{87}Sr/^{86}Sr$) of freshwater in the Adelaide River is due to the nature and age of the bedrock (and its weathering products) of the river catchments (Clark & Fritz 1997). Indeed, Sr is easily leached (partially dissolved) out of the bedding rock and remains largely in solution in water (de Caritat et al. 2023). The Adelaide River floodplain consists predominantly of silt and clay and ferruginous duricrust, formed in the early Cenozoic through weathering and alteration of the basement rocks. The basement rocks of the river catchment are to the north (seaward) cretaceous claystones, mudstones, and shales (part of the widespread Darwin Formation), which unconformably overlay the variably metamorphosed Paleoproterozoic (>1.8 giga annum [Ga]) sediments that form the southern part of the Adelaide River catchment (Doyle & Lally 2004). These Paleoproterozoic formations include variably metamorphosed sandstones, shales, siltstones, and felspar-rich greywackes. These Paleoproterozoic formations are unconformably overlaid on Neoarchaean granitic basement (≈2.6–2.8 Ga; Lally & Worden 2004). These lithologies are rich in high Rb/Sr minerals easily weathered, such as micas and feldspar. Further, the old age of these rocks (i.e. ⩾1.8 Ga) coupled with the high Rb/Sr ratio imply a long-term radioactive ingrowth of Sr, leading to a radiogenic signature (i.e. $^{87}Sr/^{86}Sr$ >0.76; de Caritat et al. 2023).

In riverine systems of the Northern Territory, Sr isotopic ratios vary significantly by season (Crook et al. 2017). These seasonal variations are influenced by runoff from the surrounding geological terrestrial inputs, which alter the isotopic composition of the river water, making it more radiogenic with increased runoff (precipitation). This is because Sr concentration and $^{87}Sr/^{86}Sr$ composition of groundwater and surface run-off are determined by the composition of host rock and soil with which they have interacted (Clark & Fritz 1997). The mixing model between seawater (higher Sr, lower $^{87}Sr/^{86}Sr$) and a dissolved crustal Sr (lower Sr, higher $^{87}Sr/^{86}Sr$ ratio) accounts for the strong compositional gradient measured at a given time along a transect of the Adelaide River (compositional snapshot) (Figs. 4 & 5). However, the shape and extent of this isotopic Sr gradient on an annual scale will depend mostly on precipitation at the time of sampling. The rainfall pattern in the study area is extremely contrasted across the year. The wet season may cumulate ~2000 mm of rain during November–April, while precipitation is near zero during the dry season (<20 mm from May to October).

The Sr isotopic front shifts downstream during the wet season (Fig. 5), depending on the amount of freshwater added to the system and its DCSr content, i.e. the extent to which radiogenic Sr is leached from the surrounding rocks within the wider river catchment (Crook et al. 2017, de Caritat et al. 2023). De Caritat et al. (2023) reported $^{87}Sr/^{86}Sr$ ratios of 0.7295–0.7405 in the lower catchment and 0.7922–1.0330 in the upper catchment regions, both of which differ significantly from the mean global $^{87}Sr/^{86}Sr$ runoff (0.7119), and the global marine $^{87}Sr/^{86}Sr$ value of 0.7092 (Veizer 1989). In contrast, during the dry season, (1) reduced terrestrial outflow leads to increased marine ingress, pushing marine Sr (with a lower $^{87}Sr/^{86}Sr$) upstream, and (2) as surface runoff diminishes to negligible levels (proportionate to precipitation), discharge into the riverine system is dominated by groundwater associated primarily with the Koolpinyah and Coomalie Dolostone aquifers and surrounding limestone formations (Haiblen et al. 2020). These formations, which contain low rubidium, impart a less radiogenic Sr signature in groundwater, resulting in lower $^{87}Sr/^{86}Sr$ values during the dry season. Cumulatively, this results in high Sr content and low $^{87}Sr/^{86}Sr$ values (approaching marine) in the dry season. This large-amplitude seasonal effect was documented by Crook et al. (2017) in the Daly River, located <100 km southwest of the Adelaide River, and is illustrated accordingly for the Adelaide River (Fig. 5) to provide a baseline for discussing the variability of Sr elemental and isotopic compositions of the *G. glyphis* vertebrae, and similar principles can be inferred for patterns observed in the *G. garricki* vertebrae where annual precipitation patterns are similarly pronounced.

4.3. Temporal validation of Sr bands through $^{87}Sr/^{86}Sr$ characterisation

The present examination of calcified hard parts from stenohaline marine species provided strong evidence that the ambient marine $^{87}Sr/^{86}Sr$ ratio is incorporated into calcified structures in ratios consistent with the ambient environment. When this finding is applied to *G. glyphis* living in an estuarine environment with a seasonally dynamic Sr profile, it provides a sound basis to examine changes in $^{87}Sr/^{86}Sr$ along the vertebral growth axis and to link these changes to environmental processes influencing this ratio, i.e. in the present case, rainfall patterns associated with the region's pronounced wet and dry seasons. For *G. glyphis*, changes in Sr concentration and $^{87}Sr/^{86}Sr$ values along the growth axis indicate close alignment with the Sr bands, and do not always align with visible band pairs. The Sr banding is driven by annual changes in Sr; in the wet season when rainfall is high and marine water intrusion is reduced, the ambient Sr concentration is low although the $^{87}Sr/^{86}Sr$ ratio is higher. In the dry season when marine water intrusion is higher and rainfall is negligible, the ambient Sr concentration is high and $^{87}Sr/^{86}Sr$ ratio is lower. Collectively, the Sr isotope characterisation along the growth transect of the vertebrae suggests that the Sr bands observed through μXRF are indicative of the number of wet and dry seasons the individual has experienced and are thus more indicative of age as opposed to visible bands that were found to not correspond to rainfall seasonality.

The $^{87}Sr/^{86}Sr$ signature is inversely correlated to Sr concentration, echoing the measured and modelled variation of the river water composition; as Sr concentration decreased, there was a correlated rise in $^{87}Sr/^{86}Sr$ values, corresponding with the pluvial maximum of the wet season (Fig. 7). The $^{87}Sr/^{86}Sr$ variation mimics the rainfall pattern to such temporal detail/resolution that recognition of multiple precipitation peaks of different heavy precipitation periods within the same wet season was possible (e.g. 2011–2012, 2012–2013 in ID9, ID10; Fig. 7). The illustrated link between rainfall and *in situ* $^{87}Sr/^{86}Sr$ values also notably implies that the environmental Sr conditions are incorporated into the vertebrae with little time lag. Therefore, given the dynamic of Sr composition in the Adelaide River, imparted by the seasonality of the rainfall, the distance between minima and maxima of the isotopic and elemental Sr record, respectively, is equivalent to 1 year along the growth axis. The significance is that these $^{87}Sr/^{86}Sr$ fluctuations match the Sr bands observed in μXRF, and are anchored to time via the recorded temporal precipitation record. This validates the temporal periodicity of Sr band pair formation as annual and invalidates the annual formation of visible band pairs in this species, which do not appear to show a consistent formation pattern across time. These implications are discussed in Section 4.4.

From what is understood of *G. glyphis* life history, juveniles and subadults tend to remain within a tight salinity niche within the estuary over prolonged periods (Pillans et al. 2009, Dwyer et al. 2020, Grant et al. 2023). There is a lack of knowledge about habitat use by larger adults (White et al. 2015, Constance et al. 2024); however, elemental analysis from a single adult male in southern Papua New Guinea indicated that it primarily used lower estuarine environments

encroaching on marine in later life phases, which matched element concentrations in the pre-natal zone of other individuals examined, indicating lower estuary use by pregnant females (Grant et al. 2023). For *G. glyphis* and *G. garricki* in the present study, $^{87}Sr/^{86}Sr$ ratios in the pre-natal section of the vertebrae show homogeneous composition with strong marine influence averaging 0.7107, supporting the suggestion of Grant et al. (2023) on the use of the lower estuary by pregnant females. Both species also exhibit a low-intensity Sr band immediately after the birthmark (and $^{87}Sr/^{86}Sr$ was higher, e.g. Fig. 6), indicating that pupping occurred at the early onset of the wet season, accordant with field observation of the pupping season in Australia and Papua New Guinea (October–December; Pillans et al. 2009, Grant et al. 2021). Taken together, this suggests that mating is likely occurring in the late wet season or early dry season, with gestation occurring through the ~8 mo dry season period before pupping in the early wet season. The caveat to this interpretation is that physiological processes of elemental uptake during the pre-natal period are unclear and may differ from post-natal uptake (Raoult et al. 2018). However, Grant et al. (2023) presented evidence that elemental reconstructions across pre- and post-natal life phases match observational data, with Sr:Ba ratios reflecting the catadromous-like pupping and early freshwater use by largetooth sawfish *Pristis pristis*. The growing evidence is that examination of passively absorbed elements such as Sr can be used to make inferences about habitat use patterns of pregnant females via patterns in the pre-natal zone of vertebrae, although this is not the case for more dietary absorbed elements like Zn (Raoult et al. 2018).

Due to the magnitude of change in the vertebral $^{87}Sr/^{86}Sr$ values and the trends with ontogeny, it appears these individuals do not spend extended periods of time within extreme freshwater areas. In most cases, the oldest individuals show a pattern of decreasing amplitude in $^{87}Sr/^{86}Sr$ and Sr peaks with age, accompanied by an overall trend towards marine values. We interpret this trend as a change in behaviour when larger *G. glyphis* individuals spend more time in lower estuarine waters more dominated by marine influence, likely due to a greater need for ecological space in lower estuarine or coastal outflow areas by larger size classes (Grant et al. 2019). However, individuals with age estimates up to 11 yr (approximate sexual maturity) still retained a Sr banding pattern in μXRF images, and discernible fluctuations in $^{87}Sr/^{86}Sr$ values, when compared to *Carcharhinus coatesi* from an inshore marine environment adjacent to the Adelaide River. This matches the limited observational data that larger subadult and adult *Glyphis* spp. may only be transient in marine environments (Pillans et al. 2009, White et al. 2015, Kyne et al. 2021b) and that their primary ecological range does not appear to overlap with inshore marine species (Grant et al. 2023).

4.4. Implications for age determination

This study has provided a robust indication that for speartooth sharks in the Adelaide River, Sr band pairs are more indicative of age than visible band pairs. These results add further evidence to the varied applicability of age estimation through counting visible band pairs under TLOM (Harry 2018, Natanson et al. 2018, Burke et al. 2020, James & Natanson 2021). The presence of visible bands does not appear to consistently reflect seasonality in the *G. glyphis* vertebrae and raises questions about the physiological processes leading to their formation. A confusing trait of visible banding is that even in species where bands are present but not correlating to time (i.e. age), larger individuals tend to have a greater number of band pairs, and vertebral centra themselves become larger with body size (e.g. Natanson & Cailliet 1990, Natanson et al. 2018, James & Natanson 2021). While the physiological processes driving the formation of bands are unclear, there are suggestions that accretion in vertebrae may rather have closer correlations to somatic growth, body shape, and ultimately structural morphometrics, rather than time (for further discussion, see Natanson et al. 2018). In the context of ongoing investigation into the reliability of age estimation through vertebral band pair counts, the present study suggests some agreement (5/9 individuals) in visible banding age estimates through TLOM with Sr ages. However, the positioning of these bands along the vertebral growth axis that was identified between methods often did not align, and age estimates between methods may have differed if these individuals were aged at alternative sizes. Formation of visible bands identified with TLOM appears to be driven by a process not directly related to wet and dry seasons, and may only be coincidentally aligning with the Sr ages in some stages of growth (e.g. Fig. 2). The present study adds *G. glyphis* to the growing evidence base that visible band pairs are not precisely indicative of time; however, it also indicates that visible bands can be broadly indicative of age when validation methods are not possible. The ongoing uncertainty in the field of ageing elasmobranchs is that for

certain species, visible band pair depositions have been demonstrated to be annually formed, particularly in earlier age classes (e.g. Simpfendorfer et al. 2002). The contention is whether, in these instances, annual band pair formation is a function of an annual process within the ambient environment such as seasonal temperature fluctuations as traditionally thought (Goldman & Cailliet 2004), or a function of somatic growth and associated structural morphometrics that correspond to seasonal change in some instances (Natanson et al. 2018). This underlines the need to validate the temporal periodicity of band pair formation within age and growth studies.

The results of the present study corroborate its central hypothesis, that predictable seasonal changes in $^{87}Sr/^{86}Sr$ ratios (and Sr concentration) within a riverine environment could be detected within calcified hard parts of a shark living in that riverine environment. It is notable that Sr isotopes in vertebrae of marine species (Australian blackspot shark) indicate that Sr from terrigenous runoff has extremely minimal to no influence on the $^{87}Sr/^{86}Sr$ composition of marine environments, as was somewhat expected. These results suggest that the use of $^{87}Sr/^{86}Sr$ ratio and its association with terrestrial runoff toward age validation in stenohaline marine species does not appear to be effective. However, for estuarine generalist species (Grant et al. 2019) with lower associations to freshwater than *G. glyphis* (a euryhaline generalist, which is considered to have higher tolerance to freshwater; Grant et al. 2019), Sr may be a useful means of age validation. For example, Scharer et al. (2012) found that the relationship between ambient elemental Sr concentration and salinity fluctuations in response to rainfall was reflected in Sr:Ca ratios within vertebrae of juvenile smalltooth sawfish *Pristis pectinata*, allowing validation of band pairs for age classes 0–3. For non-marine elasmobranchs (see species lists provided by Grant et al. 2019), the present indication is that characterisation of elements and isotopes with known relationships to terrestrial runoff offer a means of validated age estimation, while it appears to be unsuitable for stenohaline marine species.

For species only occurring within marine environments, other elements and isotopes that fluctuate predictably with season need to be identified and explored in the context of ageing. However, one consideration is the detectability of trace elements alternative to Sr, which is a highly abundant trace element within vertebrae. High-resolution *in situ* LA-ICP-MS mapping is a promising method to overcome this constraint, as challenges remain in detectability of low-concentration trace elements through μXRF imagery. Another consideration is the increased movement potential of species in marine environments, which may be a complicating factor for the use of environmental trace elements and isotopes, particularly for wide-ranging species (Raoult et al. 2016).

While the characterisation of elements and isotopes proved useful for ageing juvenile and subadult age classes in the present study, this technique may also encounter 'missing time' issues (a lack or absence of material being accreted in vertebrae) for adults approaching maximum size, as observed in TLOM methods (Harry 2018). The premise of using marine environmental chemistry to improve maximum age estimation has already been partly explored through bomb radiocarbon (^{14}C) methods (Hamady et al. 2014, Andrews & Kerr 2015). However, precise ageing of annual cohorts through ^{14}C is hampered by the necessity for local reference material, low concentration (and detectability), and contamination with natural sources of ^{14}C (e.g. Natanson et al. 2006). It may be necessary to combine age estimation methods using both validated band pair counts and bomb radiocarbon, to most accurately estimate ages up to and closely beyond sexual maturity, and maximum age, respectively. While further research is still required to determine the applicability of elemental and isotopic characterisation toward age estimation of adults approaching maximum size, what this study has shown is that environmental and seasonally controlled and predictable elemental and isotopic variations offer the possibility to enhance and support more accurate and precise age estimation.

5. CONCLUSIONS

The study species, high seasonality of the study site, and previous research indicating a strong $^{87}Sr/^{86}Sr$ signature in the host geology provided an ideal set of circumstances to test the hypothesis that environmental elements and their isotopes that have predictable seasonal fluctuations could be used to estimate age within calcified hard parts of a chondrichthyan species. This was successfully achieved and adds to the evidence base that traditional use of visible band pairs requires validation and band pairs should not be assumed to represent annual growth. The finding that ^{87}Sr and ^{86}Sr are incorporated into calcified hard parts at a ratio approximately equal to the ambient value additionally extends our knowledge about passive isotope uptake (e.g. minimal fractionation) and accretion in calcified hard parts of chondrichthyans. Modern analytical platforms have

increased capacity to make high-resolution *in situ* measurements of elemental and isotopic compositions, and these complementary advances in analytical capacity should continue to be explored. Overall, the findings of this study have very positive implications for future work aimed at more precisely understanding life histories and ecology of chondrichthyans. Applying advanced analytical techniques with higher resolving power, both spatially and analytically, including elemental maps produced by LA-ICP-MS, would benefit this field and greatly complement continued efforts by conventional approaches such as ageing by TLOM. Future research in different localities, and cumulative observations for species and elements across habitat types (coastal, pelagic, deep-water) will assist in determining the ultimate viability and limitations of the application developed herein.

Animal ethics. All *Glyphis glyphis* samples were collected with approval from the Charles Darwin University Animal Ethics Committee (approval numbers A11041 and A19008) and undertaken through Northern Territory Fisheries Act Special Permits S17/3364 and S17/3467. The *Carcharhinus falciformis* sample was collected with permission from traditional landowners and imported to James Cook University under BIOCON permits 0002424804 and 0004378941 issued by the Department of Agriculture, Water, and Environment. *Carcharhinus coatesi* were collected under Section 17 of the Northern Territory of Australia Fisheries Act. The *Squalus megalops* samples were obtained from the bycatch of commercial prawn trawlers operating in the Queensland East Coast Otter Trawl Fishery under James Cook University Ethics Approval A1566, Great Barrier Reef Marine Park Authority Permit G10/33603.1, and Department of Fisheries, Agriculture and Forestry Permits 55105 and 147714. The *Glyphis garricki* sample was collected under Western Australia Fish Resources Management Act 1994 Section 7 2(a) Exemption number 3311 with a scientific use licence held by the Department of Primary Industries and Regional Development.

Acknowledgements. We thank the Save Our Seas Foundation for funding this study, and the Macquarie University GeoAnalytical Facilities and the Advanced Analytical Centre at James Cook University for facilitating analyses. We thank Dr. Alex McCoy-West for his assistance and knowledge that facilitated this study. For collection of samples used in this study, we thank Traditional Owners, field assistants, Australia Bay Seafood Company, Dr. Cassandra Rigby, Dr. William White, Dr. Leontine Baje, the Papua New Guinea National Fisheries Authority, and the Australian Centre for International Agricultural Research. This study was funded by the Save Our Seas Foundation Small Grant #576. *Glyphis glyphis* sample collection was supported by the Marine Biodiversity Hub, a collaborative partnership supported through funding from the Australian Government's National Environmental Science Program. Adelaide River water sample collection was funded and completed by P.M.K. This study was further supported by a grant from Australia and Pacific Science Foundation (*APSF*24035) to O.A. and H.M.K.L., and by a *Future* grant from the Australian National University to O.A.

LITERATURE CITED

Andrews AH, Kerr LA (2015) Validated age estimates for large white sharks of the northeastern Pacific Ocean: altered perceptions of vertebral growth shed light on complicated bomb $\Delta^{14}C$ results. Environ Biol Fishes 98: 971–978

Burke PJ, Raoult V, Natanson LJ, Murphy TD, Peddemors V, Williamson JE (2020) Struggling with age: common sawsharks (*Pristiophorus cirratus*) defy age determination using a range of traditional methods. Fish Res 231:105706

Cailliet GM (2015) Perspectives on elasmobranch life-history studies: a focus on age validation and relevance to fishery management. J Fish Biol 87:1271–1292

Cailliet GM, Radtke R (1987) Age verification techniques in elasmobranchs: a progress report on electron microprobe analysis. In: Summerfelt RC, Hall GE (eds) The age and growth of fish. Iowa State University Press, Ames, IA, p 359–369

Cailliet GM, Smith WD, Mollet HF, Goldman KJ (2006) Age and growth studies of chondrichthyan fishes: the need for consistency in terminology, verification, validation, and growth function fitting. Environ Biol Fishes 77:211–228

Campana SE (2001) Accuracy, precision and quality control in age determination, including a review of the use and abuse of age validation methods. J Fish Biol 59:197–242

Charlier B, Ginibre C, Morgan D, Nowell G, Pearson D, Davidson J, Ottley C (2006) Methods for the microsampling and high-precision analysis of strontium and rubidium isotopes at single crystal scale for petrological and geochronological applications. Chem Geol 232:114–133

Chew D, Drost K, Marsh J, Petrus J (2021) LA-ICP-MS imaging in the geosciences and its applications to geochronology. Chem Geol 559:119917

Clark ID, Fritz P (1997) Environmental isotopes in hydrogeology. CRC Press, Boca Raton, FL

Constance JM, Garcia EA, Pillans RD, Udyawer V, Kyne PM (2024) A review of the life history and ecology of euryhaline and estuarine sharks and rays. Rev Fish Biol Fish 34:65–89

Cortés E (2000) Life history patterns and correlations in sharks. Rev Fish Sci 8:299–344

Cortés E, Grant MI, Dureuil M, Ellis JR (2024) Life history characteristics. In: Jabado RW, Morata AZA, Bennett R, Finucci B and others (eds) The global status of sharks, rays, and chimaeras. IUCN/SSC Shark Specialist Group, IUCN, Gland, p 33–38

Crook DA, Lacksen K, King AJ, Buckle DJ and others (2017) Temporal and spatial variation in strontium in a tropical river: implications for otolith chemistry analyses of fish migration. Can J Fish Aquat Sci 74:533–545

de Caritat P, Dosseto A, Dux F (2023) A strontium isoscape of northern Australia. Earth Syst Sci Data 15:1655–1673

Doyle NJ, Lally JH (2004) Noonamah, Northern Territory. 1: 100000 geological map series explanatory notes, 5172. Northern Territory Geological Survey, Darwin

Dwyer RG, Campbell HA, Cramp RL, Burke CL and others (2020) Niche partitioning between river shark species is driven by seasonal fluctuations in environmental salinity. Funct Ecol 34:2170–2185

Goldman K, Cailliet G (2004) Age determination and validation in chondrichthyan fishes. In: Carrier JC, Musick JA,

Heithaus M (eds) Biology of sharks and their relatives, Vol 2. CRC Press, Boca Raton, FL, p 399–447

Grant MI, Cortés E (2024) Life history constraints to exploitation. In: Jabado RW, Morata AZA, Bennett R, Finucci B and others (eds) The global status of sharks, rays, and chimaeras. IUCN/SSC Shark Specialist Group, IUCN, Gland, p 38–46

Grant MI, Smart JJ, White WT, Chin A, Baje L, Simpfendorfer CA (2018) Life history characteristics of the silky shark *Carcharhinus falciformis* from the central west Pacific. Mar Freshw Res 69:562–573

Grant MI, Kyne PM, Simpfendorfer CA, White WT, Chin A (2019) Categorising use patterns of non-marine environments by elasmobranchs and a review of their extinction risk. Rev Fish Biol Fish 29:689–710

Grant MI, White WT, Amepou Y, Appleyard SA and others (2021) Papua New Guinea: a potential refuge for threatened Indo–Pacific river sharks and sawfishes. Front Conserv Sci 2:719981

Grant MI, Kyne PM, James J, Hu Y and others (2023) Elemental analysis of vertebrae discerns diadromous movements of threatened non-marine elasmobranchs. J Fish Biol 103:1357–1373

Haiblen AM, Symington NJ, Woltmann M, Ray A, Gow LJ, Leplastrier A, McGrath-Cohen ESB (2020) A multifaceted approach to investigating hydrogeological complexities in the Koolpinyah Dolostone Aquifer, Howard East, Northern Territory. In: Czarnota K, Roach I, Abbott S, Haynes M, Kositcin N, Ray A, Slatter E (eds) Exploring for the future: extended abstracts. Geoscience Australia, Canberra, p 1–4

Hale LF, Dudgeon JV, Mason AZ, Lowe CG (2006) Elemental signatures in the vertebral cartilage of the round stingray, *Urobatis halleri*, from Seal Beach, California. Environ Biol Fishes 77:317–325

Hall NG, Bartron C, White WT, Dharmadi, Potter IC (2012) Biology of the silky shark *Carcharhinus falciformis* (Carcharhinidae) in the eastern Indian Ocean, including an approach to estimating age when timing of parturition is not well defined. J Fish Biol 80:1320–1341

Hamady LL, Natanson LJ, Skomal GB, Thorrold SR (2014) Vertebral bomb radiocarbon suggests extreme longevity in white sharks. PLOS ONE 9:e84006

Harry AV (2018) Evidence for systemic age underestimation in shark and ray ageing studies. Fish Fish 19:185–200

Hegg JC, Kennedy BP, Fremier AK (2013) Predicting strontium isotope variation and fish location with bedrock geology: understanding the effects of geologic heterogeneity. Chem Geol 360–361:89–98

Heupel M, Simpfendorfer C, Chin A, Appleyard S and others (2020) Examination of connectivity of hammerhead sharks in northern Australia. Report to the National Environmental Science Program, Marine Biodiversity Hub. Australian Institute of Marine Science, Cape Cleveland

IUCN (2024) The IUCN Red List of Threatened Species. https://www.iucnredlist.org/

James KC, Natanson LJ (2021) Positional and ontogenetic variation in vertebral centra morphology in five batoid species. Mar Freshw Res 72:887–898

Kirke AK, Crook DA, Banks S, Luiz OJ, Saunders TM, King AJ, Johnson GJ (2024) Reproductive biology of two small-bodied sharks, *Carcharhinus coatesi* and *Rhizoprionodon acutus*, in the Northern Territory, Australia. Fish Res 272:106946

Kyne PM, Rigby CL, Darwall WRT, Grant MI, Simpfendorfer C (2021a) *Glyphis glyphis*. The IUCN Red List of Threatened Species 2021: e.T39379A68624306. https://dx.doi.org/10.2305/IUCN.UK.2021-2.RLTS.T39379A68624306.en

Kyne PM, Davies CL, Devloo-Delva F, Johnson GJ and others (2021b) Molecular analysis of newly-discovered geographic range of the threatened river shark *Glyphis glyphis* reveals distinct populations. Report to the National Environmental Science Program, Marine Biodiversity Hub, Charles Darwin University and CSIRO, Darwin

Lally J, Worden K (2004) Geochronology in the Pine Creek Orogen — new results from NTGS. In: Munson TJ, Scrimgeour I (eds) Annual Geoscience Exploration Seminar (AGES) 2004. Record of abstracts. Northern Territory Geological Survey Record 2004-001. Northern Territory Geological Survey, Darwin, p 3–4

McArthur JM, Howarth RJ, Bailey TR (2001) Strontium isotope stratigraphy: LOWESS Version 3: Best fit to the marine Sr-isotope curve for 0–509 Ma and accompanying look-up table for deriving numerical age. J Geol 109: 155–170

McFarlane GA, Beamish RJ (1987) Validation of the dorsal spine method of age determination for spiny dogfish. In: Summerfelt RC, Hall GE (eds) The age and growth of fish. Iowa State University Press, Ames, IA, p 287–300

McMillan MN, Izzo C, Wade B, Gillanders BM (2017) Elements and elasmobranchs: hypotheses, assumptions and limitations of elemental analysis. J Fish Biol 90:559–594

Mulder J, Hagen-Peter G, Ubide T, Andreasen R and others (2023) New reference materials, analytical procedures and data reduction strategies for Sr isotope measurements in geological materials by LA-MC-ICP-MS. Geostand Geoanal Res 47:311–336

Natanson LJ, Cailliet GM (1990) Vertebral growth zone deposition in Pacific angel sharks. Copeia 1990:1133–1145

Natanson LJ, Kohler NE, Ardizzone D, Cailliet GM, Wintner SP, Mollet HF (2006) Validated age and growth estimates for the shortfin mako, *Isurus oxyrinchus*, in the North Atlantic Ocean. Environ Biol Fishes 77:367–383

Natanson LJ, Skomal GB, Hoffmann SL, Porter ME, Goldman KJ, Serra D (2018) Age and growth of sharks: Do vertebral band pairs record age? Mar Freshw Res 69: 1440–1452

Phan TT, Fulton L, Ulkem J, Aiken S and others (2021) Lepidolite extraction solid by-product: mitigation of thallium leaching and utilization of radiogenic strontium isotopes as a tracer. Environ Adv 3:100035

Pillans RD, Stevens JD, Kyne PM, Salini J (2009) Observations on the distribution, biology, short-term movements and habitat requirements of river sharks *Glyphis* spp. in northern Australia. Endang Species Res 10:321–332

Raoult V, Peddemors VM, Zahra D, Howell N, Howard DL, De Jonge MD, Williamson JE (2016) Strontium mineralization of shark vertebrae. Sci Rep 6:29698

Raoult V, Howell N, Zahra D, Peddemors VM and others (2018) Localized zinc distribution in shark vertebrae suggests differential deposition during ontogeny and across vertebral structures. PLOS ONE 13:e0190927

Rigby CL, Daley RK, Simpfendorfer CA (2016) Comparison of life histories of two deep-water sharks from eastern Australia: the piked spurdog and the Philippine spurdog. Mar Freshw Res 67:1546–1561

Scharer RM, Patterson WF III, Carlson JK, Poulakis GR

(2012) Age and growth of endangered smalltooth sawfish (*Pristis pectinata*) verified with LA-ICP-MS analysis of vertebrae. PLOS ONE 7:e47850

Simpfendorfer CA, McAuley RB, Chidlow J, Unsworth P (2002) Validated age and growth of the dusky shark, *Carcharhinus obscurus*, from Western Australian waters. Mar Freshw Res 53:567–573

Smith WD, Miller JA, Heppell SS (2013) Elemental markers in elasmobranchs: effects of environmental history and growth on vertebral chemistry. PLOS ONE 8:e62423

Tillett BJ, Meekan MG, Parry D, Munksgaard N, Field IC, Thorburn D, Bradshaw CJA (2011) Decoding fingerprints: elemental composition of vertebrae correlates to age-related habitat use in two morphologically similar sharks. Mar Ecol Prog Ser 434:133–142

Veizer J (1989) Strontium isotopes in seawater through time. Annu Rev Earth Planet Sci 17:141–167

Vroon PZ, Van Der Wagt B, Koornneef JM, Davies GR (2008) Problems in obtaining precise and accurate Sr isotope analysis from geological materials using laser ablation MC-ICPMS. Anal Bioanal Chem 390: 465–476

White WT, Appleyard SA, Sabub B, Kyne PM and others (2015) Rediscovery of the threatened river sharks, *Glyphis garricki* and *G. glyphis*, in Papua New Guinea. PLOS ONE 10:e0140075

Zaky AH, Brand U, Buhl D, Blamey N and others (2019) Strontium isotope geochemistry of modern and ancient archives: tracer of secular change in ocean chemistry. Can J Earth Sci 56:245–264

Editorial responsibility: Stephen Wing Dunedin, New Zealand
Reviewed by: 3 anonymous referees
Submitted: October 9, 2024; Accepted: July 17, 2025
Proofs received from author(s): October 12, 2025